COMPUTER METHODS AND PROGRAMS IN BIOMEDICINE 113 (2014) 593–609

journal homepage: www.intl.elsevierhealth.com/journals/cmpb

Robust information gain based fuzzy c-means clustering and classification of carotid artery ultrasound images

Mehdi Hassan[a], *Asmatullah Chaudhry*[b], *Asifullah Khan*[a,*], *M. Aksam Iftikhar*[a]

[a] *Pattern Recognition Lab (DCIS), PIEAS, P.O. Nilore 45650, Islamabad, Pakistan*
[b] *NDTG, PINSTECH, P.O. Nilore 45650, Islamabad, Pakistan*

ARTICLE INFO

Article history:
Received 11 July 2013
Received in revised form
26 September 2013
Accepted 15 October 2013

Keywords:
Decision system
Image segmentation
Information gain
Fuzzy c-means clustering
Probabilistic neural networks
Carotid artery

ABSTRACT

In this paper, a robust method is proposed for segmentation of medical images by exploiting the concept of information gain. Medical images contain inherent noise due to imaging equipment, operating environment and patient movement during image acquisition. A robust medical image segmentation technique is thus inevitable for accurate results in subsequent stages. The clustering technique proposed in this work updates fuzzy membership values and cluster centroids based on information gain computed from the local neighborhood of a pixel. The proposed approach is less sensitive to noise and produces homogeneous clustering. Experiments are performed on medical and non-medical images and results are compared with state of the art segmentation approaches. Analysis of visual and quantitative results verifies that the proposed approach outperforms other techniques both on noisy and noise free images. Furthermore, the proposed technique is used to segment a dataset of 300 real carotid artery ultrasound images. A decision system for plaque detection in the carotid artery is then proposed. Intima media thickness (IMT) is measured from the segmented images produced by the proposed approach. A feature vector based on IMT values is constructed for making decision about the presence of plaque in carotid artery using probabilistic neural network (PNN). The proposed decision system detects plaque in carotid artery images with high accuracy. Finally, effect of the proposed segmentation technique has also been investigated on classification of carotid artery ultrasound images.

1. Introduction

Image segmentation is the process of grouping pixels of an image into several homogeneous regions. It finds various applications in many practical computer vision tasks like object tracking, pattern recognition, image classification, disease diagnostics using medical imaging.

In image segmentation, nature of the image under study and its intrinsic degradations may pose severe challenges to the process of segmentation. For instance, in medical imaging, ultrasound images are corrupted by speckle noise and wave interference which may degrade the segmentation quality.

Disease diagnosis based on medical imaging is an invaluable tool for medical experts to plan a patients' rehabilitation process. Several imaging modalities are available to medical practitioners, including ultrasound imaging, magnetic resonance imaging (MRI), computed tomography (CT), and digital mammography, which help them diagnosing the disease

* *Corresponding author*. Tel.: +92 51 2207381 3; fax: +92 51 2208070.
E-mail addresses: asif@pieas.edu.pk, khan.asifullah@gmail.com (A. Khan).
0169-2607/$ – see front matter
http://dx.doi.org/10.1016/j.cmpb.2013.10.012

accurately in a non-invasive way. However, as the volume of medical images has grown exponentially, therefore, analyzing and interpreting of these images manually is no more feasible. A computer aided diagnostic (CAD) system is highly desirable to provide additional support to the radiologists. Particularly, effective computer algorithms are required to illustrate the structures and region of interest (ROI) automatically. These algorithms usually segment a medical image into its constituent structures (regions) and play a significant role in various medical image analysis tasks such as quantification of tissue volume [1], diagnosis [2], anatomical structure study [3], treatment planning [4], and computer aided surgery [5]. Several methods have been proposed in the literature to segment medical images [6–14]. Each method has its own benefits and limitations. Further, there is no single segmentation technique capable of addressing all the problems simultaneously.

Fuzzy c-means (FCM) is an unsupervised fuzzy segmentation technique, which has been successfully applied in fields such as medical imaging, geology, astronomy and object recognition [4,5,15]. In FCM, clusters are obtained iteratively by minimizing a cost function which depends on the distance of pixels to the cluster centers. Each pixel may belong to more than one clusters with certain degrees of membership [16]. Therefore, it is especially useful in medical image segmentation where objects in the images do not have well-separated boundaries.

FCM performs well for segmentation of medical images but it is highly sensitive to noise which adversely affects the clustering accuracy. Moreover, FCM may produce non-homogeneous clustering in presence of noise. To overcome the lack of robustness in FCM, Chuang et al. [17] incorporated the spatial context into basic FCM framework. They conjectured that high pixels correlation present in most images can be exploited to produce more homogeneous segmentation. Their proposed method, namely spatial FCM (sFCM), modifies standard FCM by weighting membership of each pixel with the cluster distribution in its neighborhood. The sFCM algorithm produces better clustering compared to FCM technique. The sFCM algorithm was further investigated by Chaudhry et al. [2] and a modified approach was proposed for better clustering, named as spatial FCM modified (sFCMM). The sFCMM algorithm introduced a weighted similarity measure based on spatial proximity in the sFCM framework in order to produce reliable segmentation.

Cai et al. [18] have proposed a fast generalized fuzzy c-means (FGFCM) algorithm, which introduced a new similarity measure for better exploiting spatial and gray level information. The computational cost of FGFCM is dependent on the number of gray levels in the image and is typically much less than image size. Krinidis and Chatzis [15] proposed another variant of FCM, called fuzzy local information based FCM (FLICM). The main feature of FLICM is the use of yet another fuzzy similarity measure incorporating spatial and gray level local information. However, the FLICM algorithm is associated with high computational cost. Moreover, the robustness of both FLICM and FGFCM is severely affected by higher levels of noise.

All the above mentioned variants of FCM produce good enough segmentation results, but their performance depends upon some tradeoff parameter between noise removal and detail preservation.

In this paper, we intend to present an image segmentation technique, which results in homogeneous clustering even in presence of noise. The main contribution of this work is to develop a modified FCM clustering scheme, named as information gain based fuzzy c-means (IGFCM), by incorporating the concept of information gain into the basic framework of FCM. The information gain uses the concept of entropy, which has been exploited by some researchers, in different ways, in order to improve the segmentation capability in various applications [19,20]. The proposed IGFCM segmentation is a two-phase process, where phase-I of the algorithm proceeds in a way similar to classical FCM algorithm. However, contrary to saturated convergence in classical FCM, we prematurely truncate phase-I of IGFCM after completing few iterations (3–5 iterations for most applications) of FCM. The intention is to start second phase of the algorithm with a sufficiently reasonable initial estimate of the true clustering. Hence, phase-II of the proposed algorithm proceeds with output of phase-I, which updates fuzzy membership values of pixels in an informed manner. In particular, the fuzzy membership values of pixels are swapped together based on information gain for each class. Thus, the information encapsulated by information gain guides refining the segmentation process. The proposed IGFCM algorithm has been validated by segmenting images from different imaging modalities such as synthetic, daylight, CT Liver, and carotid artery ultrasound images. The performance of IGFCM has also been compared with FCM and a few other state of the art variants of FCM.

Another major contribution of this research work is development of a decision system for carotid artery ultrasound images. Therefore, it is useful to briefly overview the state of the art in decision making of carotid artery ultrasound images. Due to excessive use of cholesterol, fatty materials accumulate into the arterial wall, a condition known as atherosclerosis. The accumulation of such materials gives rise to plaques inside the artery, which blocks blood flow into the brain. The blockage due to the plaque in carotid artery may cause a cerebrovascular accident (stroke). Cerebrovascular is fourth leading cause of deaths in United States [21]. The *Ischemic* stroke occur due to the blockages such as clot or presence of plaque in carotid artery [22]. Moreover, a brain stroke may occur, if some components of plaque approach the brain due to a prospective rupture into these plaques. Therefore, it is highly desirable to detect plaque in the early stage of its development.

Currently, plaque in the artery is detected through carotid angiography. But, this involves the uncomfortable and risky process of X-ray dye injection and examination through invasive X-ray imaging. Moreover, allergic reactions and kidney failure are also potential side effects of X-ray imaging techniques.

Ultrasound imaging is a popular non-invasive tool being used for carotid artery plaque detection. However, lower quality, presence of speckle noise and wave interferences are the limitations associated with ultrasound imaging. Moreover, plaque detection and manual extraction of carotid artery contour is a tedious and subjective task. Therefore, a computer assisted diagnostic system is highly desirable in order to automatically analyze the carotid artery ultrasound images. Such a decision system will also help radiologists to establish a secondary opinion regarding the presence and severity of plaque in the carotid artery [6,11].

For successful detection of plaques in carotid artery ultrasound images, an effective segmentation is highly desirable. The desired output of segmenting a carotid artery ultrasound image is delineation of arterial walls. Segmentation of carotid artery ultrasound images prior to automatic plaque detection is useful for better judgment of normal and abnormal subjects. The carotid lumen, for example, has been extracted by a technique proposed by Mao et al. [23]. They used deformable models, which need to be initialized manually. Similarly, Loizou et al. [24] employed a user-initialization based snake model for carotid artery image segmentation. Improper initialization by naive users, may yield incorrect results while using these techniques.

Similarly, Hassan et al. [25] have proposed a segmentation technique and a corresponding decision making system, based on the proposed segmentation scheme for carotid artery plaque detection. They have proposed spatial fuzzy c-means modified (sFCMM) along with ensemble clustering on genetically reduced feature set extracted from the gray level co-occurrence matrix (GLCM), moments of gray level histogram (MGH) and 2-D continuous wavelet transform. However, their technique works well only with lower levels of noise.

Tsiaparas et al. [26] used multi-resolution techniques for texture classification of ultrasound Carotid Atherosclerosis tissue. They employed four decomposition techniques and several basis functions in order to identify asymptomatic and symptomatic cases. For each type of decomposition, the mean and standard deviation of sub-images were used as features and input to Support Vector Machines (SVM) and Probabilistic Neural Networks (PNN) classifiers. The wavelet packets decomposition technique in combination with SVM produced highest decision accuracy.

Latifoglu et al. [14] proposed a robust decision system for diagnosing atherosclerosis using carotid artery Doppler signals. Their proposed approach involves feature extraction based on Fast Fourier Transform (FFT), and feature reduction using Principle Component Analysis (PCA). The reduced features are weighted using a k-nearest neighbor (k-NN) based approach. For classification, the Artificial Immune Recognition System (AIRS) classifier was applied using 10-fold cross-validation.

Similarly, Kyriacou et al. [27] extracted features from carotid ultrasound images using spatial gray level dependence matrices (SGLDM). They used ultrasound images of 1121 patients with asymptomatic internal carotid artery stenosis (ACS) and showed that combination of SGLDM features with clinical features improves stroke prediction due to high risk plaques. SVM and PNN were used as classifier in their decision system. However, best decision accuracy was obtained by SVM classifier with SGLDM features.

In this research work, we have run the proposed IGFCM technique for segmentation of 300 real carotid artery ultrasound images. the improved segmentation helps in the proposed classification of the same images. In particular, the decision system is based on PNN classifier. A feature set, comprising 6 features, is formed using IMT values which are measured from images segmented by the proposed IGFCM technique. This feature set is fed to the PNN classifier to identify normal or abnormal subjects. We speculate that due to high-quality segmentation yielded by the proposed segmentation technique, the decision accuracy should be high. This has been verified by segmenting the 300 carotid artery images with different segmentation techniques including the proposed IGFCM algorithm. Then, these images have been classified using different classifiers. Higher classification accuracy has been obtained corresponding to images segmented by the proposed algorithm, which verifies the positive influence of the proposed IGFCM algorithm on classification process.

Rest of the paper is organized as follows. Section 2 describes the proposed scheme. Experimental results and discussion are presented in Section 3. Finally, the research is concluded and future directions are set in Section 4.

2. Materials and methods

In this section, first we briefly describe the data sets used in this research work and then describe the proposed IGFCM algorithm in detail.

2.1. Datasets

The proposed scheme in this paper is validated in two scenarios. In the first scenario, it is applied to general imaging modalities for clustering purpose. These include synthetic, daylight, liver CT images, respectively. While the second scenario deals with segmentation and decision making of carotid artery ultrasound images. The dataset, used in the second scenario, was obtained from Shifa International Hospital, Islamabad, Pakistan. Toshiba's Xario XG ultrasound machine equipped with Linear Probe transducer, having a frequency range of 7–8 MHz, has been used in the said hospital for carotid artery ultrasound imaging. The ultrasound scan videos have been recorded for 10 s each and converted into separate frames employing a video Decompiler. Original images have dimension of 800 × 600 with resolution of 72 pixels per inch (PPI). A dataset of 300 (140 normal and 160 abnormal) images has been developed to test the performance of the proposed approach. The age of the patients in the dataset varies from 35 to 74 years. Overall mean and standard deviation of age for the whole dataset are 55.75 and 9.43 years, respectively. The obtained images have been categorized into normal and abnormal with the help of medical experts. All computations are performed on an Intel Core i7 Pc with Matlab 7.12 (2011a).

2.2. Fuzzy c-means segmentation

As stated earlier, FCM assigns pixels to clusters based on their fuzzy membership values. It strives to minimize the following cost function:

$$J = \sum_{j=1}^{N}\sum_{i=1}^{C} u_{ij}^{m}||x_j - v_i||^2 \tag{1}$$

where u_{ij} shows the membership of pixel x_j to ith cluster $\forall x_j \in \Omega$, where Ω represents the set of points that an image is composed. C and N represent total number of clusters and data points in Ω, and v_i is centroid of ith cluster. The constant m is also known as degree of fuzziness and is usually set to 2 for most applications.

The cost function of FCM is minimized iteratively by updating cluster centroid. Fuzzy membership values are assigned to pixels based on their distance from the center of different clusters. The smaller the distance of pixel under consideration from cluster centroid, higher will be the degree of membership to that cluster and vice versa. The following mathematical expressions are used to update the fuzzy membership functions and cluster centers, respectively:

$$u_{ij} = \frac{1}{\sum_{k=1}^{C}(||x_j - v_i||/||x_j - v_k||)^{2/(m-1)}} \tag{2}$$

$$v_i = \frac{\sum_{j=1}^{N} u_{ij} x_j}{\sum_{j=1}^{N} u_{ij}^{m}} \tag{3}$$

2.3. *Proposed information gain based fuzzy c-means algorithm*

As described in Section 1, FCM algorithm is highly sensitive to noise and may produce non-homogeneous clustering. To handle this problem effectively, we have employed the concepts of entropy and information gain into the basic FCM algorithm. The idea of entropy was coined by Claude Shannon in his pioneering work on information theory [28]. It is the measure of uncertainty of a random variable and is calculated by the following expression.

$$\text{entropy}\,(i) = -\sum_{i} p_i \log_2 p_i, \quad \forall i \in [1, C] \tag{4}$$

where p_i is the probability of ith cluster in a certain neighborhood.

Information gain is the measure of goodness of an attribute. It is computed for a particular class using following equation:

$$IG_i = \text{entropy}\,(i) - EI, \quad \forall i \in [1, C] \tag{5}$$

EI represents expected information which is computed from available information between class entropies and their respective probabilities. The mathematical expression for *EI* is as follows.

$$EI = \sum_{i \in [1,C]} \sum_{j \in [1,C]} (p_i + p_j)\text{entropy}\,(i, j), \quad \text{where, } i \neq j \text{ and } j > i \tag{6}$$

where p_i and p_j are probabilities of cluster i and j, respectively, entropy(i,j) is the between class entropy for i and j, computed by following expression:

$$\text{entropy}\,(i, j) = -\sum_{i \in [1,C]} p_i \log_2 p_i - \sum_{j \in [1,C]} p_j \log_2 p_j \tag{7}$$

– Algorithm 1:.

Phase-I

Perform the FCM segmentation on the input image.

Compute v_{kn} (initial cluster centroids) for all k and $n \in [1,C] \times \Omega$

Compute u_{jk} (initial fuzzy membership values) for all j and $k \in [1,C] \times \Omega$

Phase-I concludes after the image is segmented by few iterations of FCM algorithm. The output of this phase is fed to Phase-II for further computation.

Phase-II

Use a 5×5 window and iterate it over the FCM segmented image. For each iteration, repeat steps 1–11.

1. Calculate the probability of each class.
$p_j = \frac{n_j}{N} \quad \forall j \in [1, C]$
where n_j represents the number of pixels in the window, which belong to class j. N is the total number of pixels (5×5) in the window.
2. Calculate the entropy of each class entropy(i) using Eq. (4).
3. Calculate the between class entropy entropy(i,j)for each two-class combination using Eq. (7).
4. Calculate expected information (*EI*) using Eq. (6).
5. Calculate information gain for each class IG_i using Eq. (5).
6. Compute $u_{jk}^{sorted} = sort(u_{jk}, \text{ORDER})$, where *sort* orders the vector u_{jk} in the order specified by ORDER. The ordered vector is returned in u_{jk}^{sorted}. We have used descending order in our algorithm.
7. Update u_{jk}^{New} using following expression:
$u_{jk}^{New} = u_{rank(IG,IG(i)),k}^{sorted} \quad \forall (j, k) \in [1, C] \times \Omega$
where *IG* sets of information gain values for all classes and *rank(IG,i)* returns the rank (i.e. order) of number *i* within a set of numbers *IG*.
8. Update v_{kn} from Eq. (3) using u_{jk}^{New}.
9. Set $u_{jk} = u_{jk}^{New}$.
10. Use u_{jk} and v_{kn} to perform FCM iteration.
11. Repeat all the above steps until the stopping criterion is met.

The proposed IGFCM algorithm is a two-phase process. In first phase, the input image is segmented by FCM for a few iterations in order to obtain an initial estimate of true segmentation. In the second phase, for each pixel in the FCM-segmented image, entropy and information gain are computed from its surrounding pixels in a certain neighborhood (5×5 selected empirically in our case). The proposed technique then updates the fuzzy membership values of a pixel by swapping them together. The swapping order of the pixel fuzzy membership values is determined by the rank of its information gain values for different clusters. The cluster centroids of the pixel are also updated, as in classical FCM. Then, an iteration of classical FCM proceeds with the new membership values and cluster centroids. This process continues until the difference between cluster centroid values in consecutive iterations reduces below a particular threshold or maximum numbers of iterations have been reached. This process is described in a step by step algorithm as follows.

The defuzzification of u_{jk} yields the final image segmented by IGFCM algorithm. Fig. 1 shows the block diagram of the proposed algorithm. A detailed illustration of above algorithmic steps is shown by an example in Fig. I-1. Note that phase-III is concerned with application of IGFCM algorithm in a classification scenario which will be described in Section 2.5.

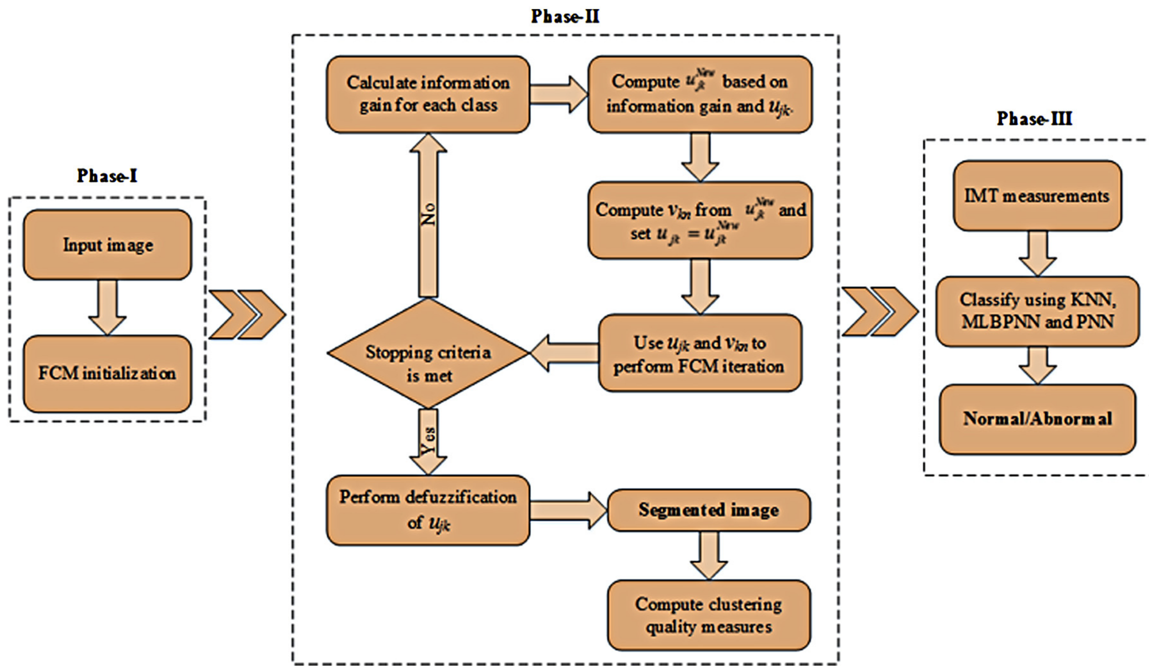

Fig. 1 – Block diagram of IGFCM.

2.3.1. *Illustration of the proposed IGFCM algorithm*

An example is presented in this section to demonstrate the working of the proposed IGFCM algorithm. Phase-I of the algorithm is simply the application of classical FCM which is well studied and can be easily applied. So, only phase-II is described in this example. We consider a local neighborhood of 5×5 pixels from the input image (FCM segmented) and apply the steps in phase-II of the proposed algorithm. These steps will be repeated for every pixel of the input image until the convergence criteria is met and the final IGFCM-segmented image is obtained. In the following text, execution of phase-II of the algorithm on a given pixel/neighborhood is presented.

Step 1. A sample local neighborhood is shown in Fig. I-1 where the pixel under consideration is shaded. Total clusters are supposed to be 5 in this case.

1	1	2	4	3
2	3	1	5	4
2	1	5	1	5
5	3	4	1	3
5	4	3	2	2

Fig. 1 – Fig. I-1. A sample pixel and corresponding local neighborhood.

The given input fuzzy membership functions in this example are as follows:

$$u_{jk} = [0.1 \quad 0.15 \quad 0.24 \quad 0.23 \quad 0.28]$$

Step 2. Calculate the probability of each class.

$$p_1 = \frac{6}{25}, \quad p_2 = \frac{5}{25}, \quad p_3 = \frac{5}{25}, \quad p_4 = \frac{4}{25}, \quad p_5 = \frac{5}{25}$$

Step 3. Calculate the entropy of each class. As an illustrative example, entropy(1) is computed as follows:

$$\text{entropy}(1) = -\frac{6}{25} \times \log_2\left(\frac{6}{25}\right) = 0.4941$$

$$\text{Therefore,} \quad \text{entropy}(i) = [0.4941 \quad 0.4644 \quad 0.4644 \quad 0.4230 \quad 0.4644], \quad \forall_i \in [1, C]$$

Step 4. Calculate the entropy between classes for each two-class combination. As an illustrative example, entropy(1,2) is computed as follows:

$$\text{entropy}(1, 2) = -\frac{6}{25} \times \log_2\left(\frac{6}{25}\right) - \frac{5}{25} \times \log_2\left(\frac{5}{25}\right) = 0.9585$$

$$\text{Therefore,} \quad \text{entropy}(i, j) = \begin{bmatrix} - & 0.9585 & 0.9585 & 0.9172 & 0.9585 \\ 0.9585 & - & 0.9288 & 0.8874 & 0.9288 \\ 0.9585 & 0.9288 & - & 0.8874 & 0.9288 \\ 0.9172 & 0.8874 & 0.8874 & - & 0.8874 \\ 0.9585 & 0.9288 & 0.9288 & 0.8874 & - \end{bmatrix}, \quad \forall (i, j) \in [1, C]$$

Step 5. Calculate expected information.

$$\begin{aligned} EI = {} & \frac{11}{25} \times \text{entropy}(1, 2) + \frac{11}{25} \times \text{entropy}(1, 3) \\ & + \frac{10}{25} \times \text{entropy}(1, 4) + \frac{11}{25} \times \text{entropy}(1, 5) \\ & + \frac{10}{25} \times \text{entropy}(2, 3) + \frac{9}{25} \times \text{entropy}(2, 4) \\ & + \frac{10}{25} \times \text{entropy}(2, 5) + \frac{9}{25} \times \text{entropy}(3, 4) \end{aligned}$$

$$+\frac{10}{25}\times \text{entropy}(3,5)+\frac{9}{25}\times \text{entropy}(4,5)$$

$$EI=\frac{11}{25}\times(0.9585+0.9585+0.9585)$$

$$+\frac{10}{25}\times(0.9172+0.9288+0.9288+0.9288)$$

$$+\frac{9}{25}\times(0.8874+0.8874+0.8874)=3.8606$$

Step 6. Calculate information gain for each class. As an illustrative example, IG_1 is computed as follows.

$$IG_1=\text{entropy}(1)-EI=0.7950-3.8606=-3.0655$$

Therefore,

$$IG=[-3.3664\quad -3.3962\quad -3.3962\quad -3.4376\quad -3.3962]$$

Step 7. Compute $u_{jk}^{sorted}=sort(u_{jk},'desc')$.

$$u_{jk}^{sorted}=[0.28\quad 0.24\quad 0.23\quad 0.15\quad 0.10]$$

Step 8. Update u_{jk}^{New}.

$$IG=[IG_1,IG_2,IG_3,IG_4,IG_5]$$

$$=[-3.3664,-3.3962,-3.3962,-3.3962,-3.4376]$$

$$\text{rank}(IG,IG_i)=\begin{bmatrix}5 & 3 & 4 & 2 & 1\end{bmatrix}$$

Therefore,

$$u_{1k}^{New}=u_{5k}^{sorted},u_{2k}^{New}=u_{3k}^{sorted}u_{3k}^{New}=u_{4k}^{sorted},u_{1k}^{New}=u_{2k}^{sorted},u_{5k}^{New}=u_{1k}^{sorted}$$

i.e. $u_{jk}^{New}=[0.28, 0.24, 0.23, 0.10, 0.15]$

Until this point, we have obtained the new fuzzy membership functions. We can use these new membership values to continue the process for further calculations (e.g. to find out new centroids as in step 9 of Phase-II).

2.4. Clustering quality measures

To evaluate the clustering performance of the proposed IGFCM and other aforementioned algorithms, following cluster quality measures have been employed.

2.4.1. Partition coefficient (PC)

Partition coefficient computes the overlap between segments [2]. It is evaluated by the following mathematical expression.

$$PC=\frac{1}{N}\left(\sum_{j=1}^{N}\sum_{i=1}^{C}u_{ij}^2\right)\tag{8}$$

Larger values of PC indicate better clustering and vice versa.

2.4.2. Classification entropy (CE)

Classification entropy is a measure of fuzziness of clusters and is computed by the following expression [2]:

$$CE=\frac{1}{N}\left(\sum_{i=1}^{C}\sum_{j=1}^{N}u_{ij}\log_2(u_{ij})\right)\tag{9}$$

Contrary to PC, smaller values of CE correspond to better clustering and vice versa.

2.5. Decision system for carotid artery ultrasound images

The segmentation performance is critical to disease diagnosis in most computer-aided diagnostic systems. Effective segmentation results in improved classification results. In this section, the impact of segmentation using the proposed IGFCM algorithm has been tested on classification of carotid artery ultrasound images. For this purpose, a decision system has been proposed based on PNN classifier. In the proposed decision system, IMT values have been measured from IGFCM-segmented carotid artery ultrasound images. The IMT values correspond to number of pixels along columns of a selected region of the segmented images which belong to the arterial wall [29,30]. Based on these measurements, a set of 6 features namely mean, variance, skewness, kurtosis, min and max [10,31] has been formed and provided as input to the classifier. Probabilistic neural network (PNN) has been employed for classification owing to better learning capability of neural networks. The use of PNN has been justified by comparing its performance with two other classifiers. Finally, the effect of segmentation has been studied by segmenting the carotid artery images with different segmentation techniques including the proposed algorithm. The dataset used in this study is described in Section 2.1.

2.5.1. Probabilistic neural networks classifier

Probabilistic neural network (PNN) is a popular and frequently used tool for decision making which works well both for nonlinear and linear data. It is a feed forward neural network based on Kernel Fisher discriminant analysis and Bayesian networks. It employs four layers of neural network namely input, hidden, pattern and output layer. Compared to multilayer perceptron, PNN is faster, more accurate and tolerant to outliers. Moreover, the complexity of the decision surface of PNN classifier can be controlled by varying the *spread* parameter. The decision surface can even approach Bayes optimal using an optimal value of the spread parameter. In our case, the spread parameter is set empirically to 0.9 to yield optimal performance. PNN classifier has capability to operate in parallel without getting feedback from individual input neurons. Finally, for time variant problems, old patterns can be replaced with new patterns. More details on PNN can be found in [32]. We have employed 10-fold cross validation using jackknife method in our experiments in order to train and validate PNN.

2.5.2. Decision performance measurements

In statistical prediction, to check the effectiveness of a method, different types of measures are used. In this work,

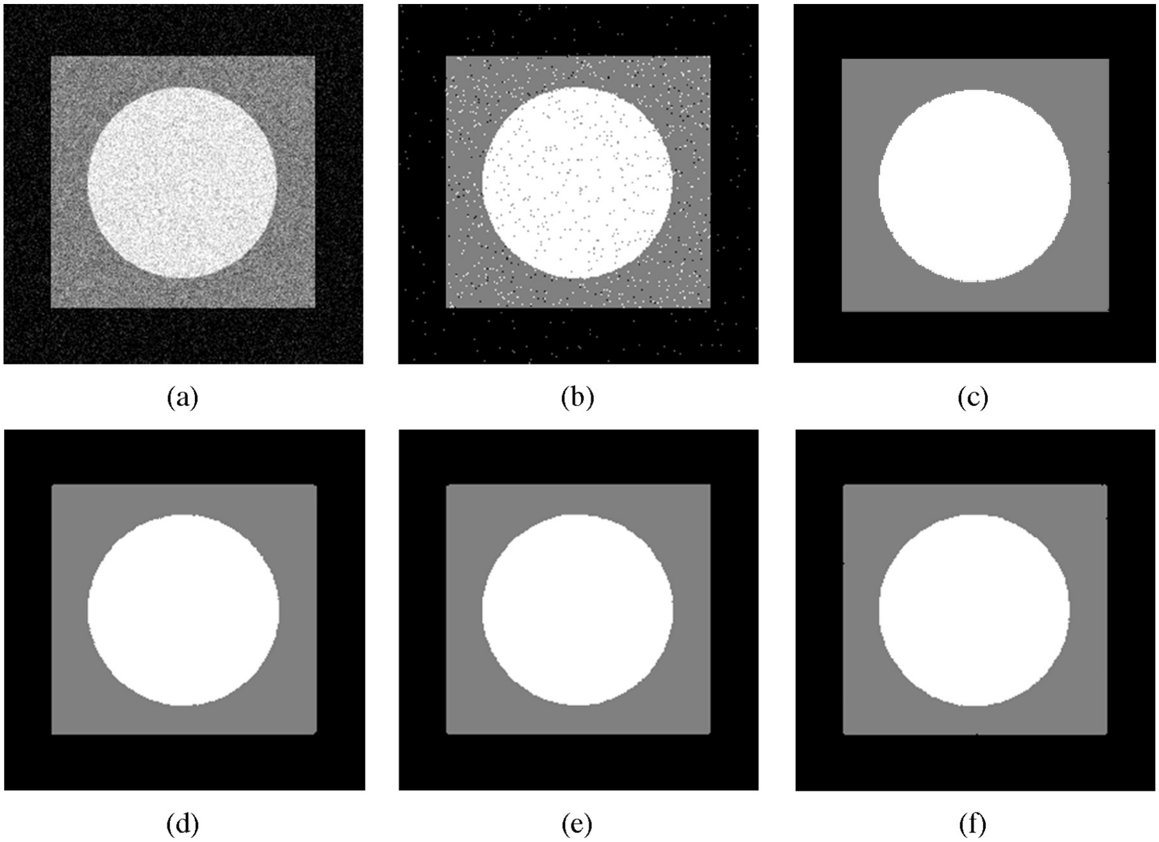

Fig. 2 – Segmentation of noisy synthetic image (noise variance 0.01): (a) noisy image segmented by (b) FCM, (c) sFCM, (d) sFCMM, (e) FLICM, and (f) the proposed IGFCM algorithm.

following measures have been computed to assess the effectiveness of classification quantitatively: accuracy, sensitivity, specificity, Mathew's Correlation Coefficient (MCC) and *F*-measure. Details of these measures can be found in [10,31].

2.5.3. *ROC and area under the curve*

The receiver operating characteristics (ROC) curve compares true positive rate against false positive rate graphically. It is used as an effective analysis tool and demonstrates how well a decision making system is performing some detection task. We have presented the performance of the proposed decision system using ROC curve. The area under the curve (AUC) [33] has also been computed from ROC curve which measures the classification performance quantitatively.

3. Experimental results and discussion

Two major experiments have been considered for validation of the proposed IGFCM segmentation technique. In experiment 1, the proposed IGFCM technique is applied to images from different imaging modalities. These images include synthetic, daylight and liver CT. The results have been obtained for both noisy and noise-free images. Performance of the proposed algorithm has been compared with standard FCM, sFCM, sFCMM and FLICM, both visually and quantitatively. Partition coefficient (PC) and classification entropy (CE) have been used as quantitative clustering performance measures.

The experiment 2 presents classification of carotid artery ultrasound images. The images have been segmented using the proposed IGFCM algorithm prior to classification so that the effect of segmentation on classification performance can be studied. The proposed decision system, based on PNN classifier, identifies carotid artery ultrasound images as normal or abnormal subjects. The use of PNN has been justified by comparing its performance with two other classifiers. A feature set has been formed based on IMT values which are measured from carotid artery ultrasound images segmented by the proposed IGFCM approach. The feature set is input to the PNN classifier in order to obtain the final decision about pathological state of the subject. A dataset of 300 real carotid artery ultrasound images is used in our decision making system (see Section 2.1). Finally, the superiority of employing the proposed IGFCM in the decision system has been shown. In particular, the carotid artery data set is segmented using different variants of FCM and used in the decision system in a way similar to IGFCM. The classification results employing different segmentation techniques verify that the proposed IGFCM technique provides improvement in classification accuracy compared to other segmentation techniques.

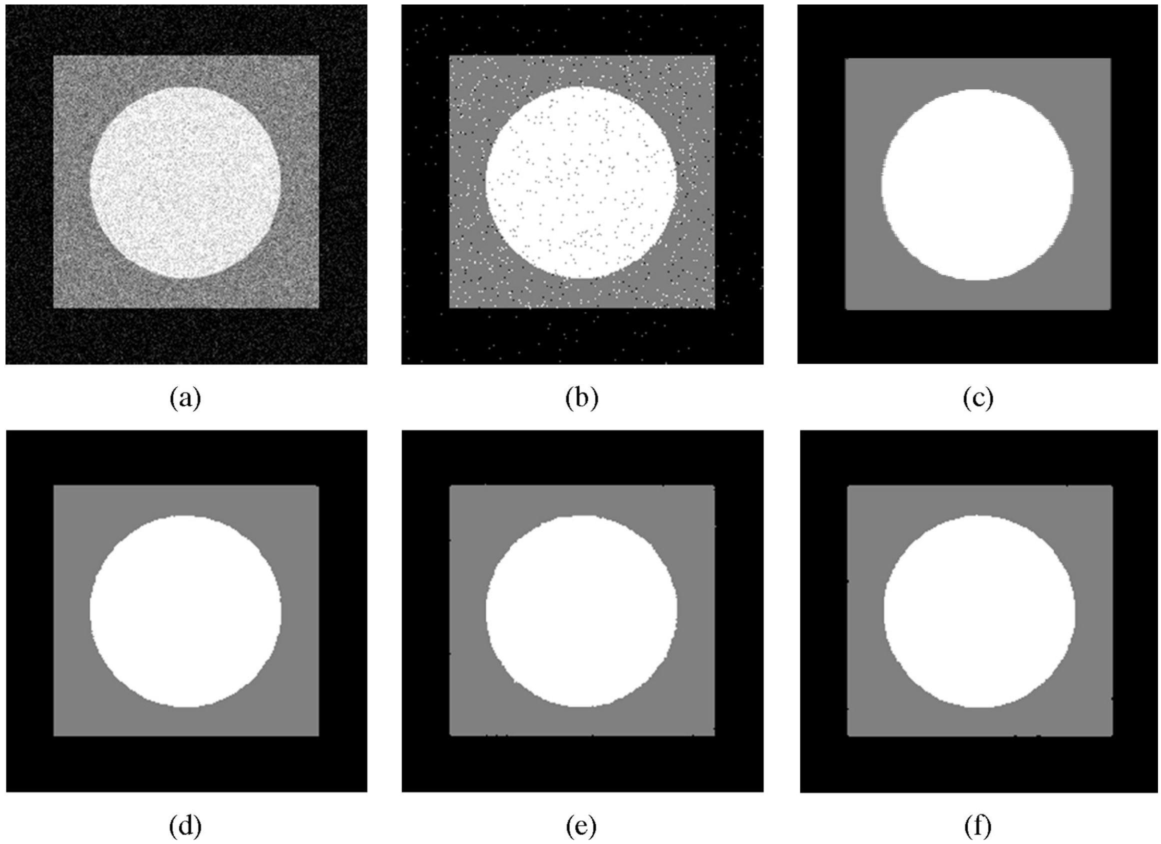

Fig. 3 – Segmentation of noisy synthetic image (noise variance 0.02): (a) noisy image segmented by (b) FCM, (c) sFCM, (d) sFCMM, (e) FLICM, and (f) the proposed IGFCM algorithm.

3.1. *Scenario 1: segmentation performance of the proposed algorithm*

In this scenario, we have applied the proposed technique for segmentation of a synthetic, daylight and CT liver image. To check the robustness to noise, images have been segmented in the presence of Gaussian noise of various intensities. Validation on images from different modalities helps verifying the general-purpose reliability of the proposed technique.

3.1.1. *Synthetic image based segmentation performance*

We first present the results of applying IGFCM and variants of FCM to a synthetic image, having three segments. Gaussian noise of different variances (0.01, 0.02 and 0.03) has been added to the image. Corresponding noisy images are shown in Figs. 2(a), 3(a) and 4(a), respectively. Figs. 2–4(b–f) show the images segmented by different techniques at various noise levels. Segmentation results obtained by IGFCM for this simple image are comparable to that of sFCM and sFCMM but clear superiority can be observed compared to FCM and FLICM algorithms at almost all noise levels. Similar conclusion is drawn from quantitative comparison of segmentation performance measures shown in Table 1.

3.1.2. *Daylight image based segmentation performance*

Daylight images also find several applications in computer vision like surveillance and object tracking. Image segmentation is an essential intermediate processing step in these applications. The performance of the proposed algorithm has been examined on a daylight image, named as 'the wolf image', which is shown in Fig. 5(a). Here, the objective is to segment the image into three logical segments. As shown in Fig. 5(b–f), the image segmented by different variants of FCM contains misclassified pixels compared to the image segmented by the proposed IGFCM algorithm. The image has also been degraded by adding Gaussian noise of variance 0.01 and different segmentation techniques have been applied to the noisy image. Fig. 6(a–f) shows noisy image and images segmented by FCM, sFCM, sFCMM, FLICM, and IGFCM, respectively. It can be observed visually that our proposed algorithm produces segmentation with minimum misclassifications. On the other hand, images segmented by standard FCM and its variants contain a lot of misclassified patterns. This verifies that IGFCM is more robust to noise and produces more homogeneous clustering compared to other segmentation techniques.

3.1.3. *CT liver image based segmentation performance*

Recognizing the importance of segmentation process in medical image analysis, the proposed IGFCM algorithm has been applied to a CT liver image (extracted region of interest) with a tumor. The proposed IGFCM algorithm, standard FCM and its variants are applied to this image. The objective is to segment the image into three clusters namely background, tumor

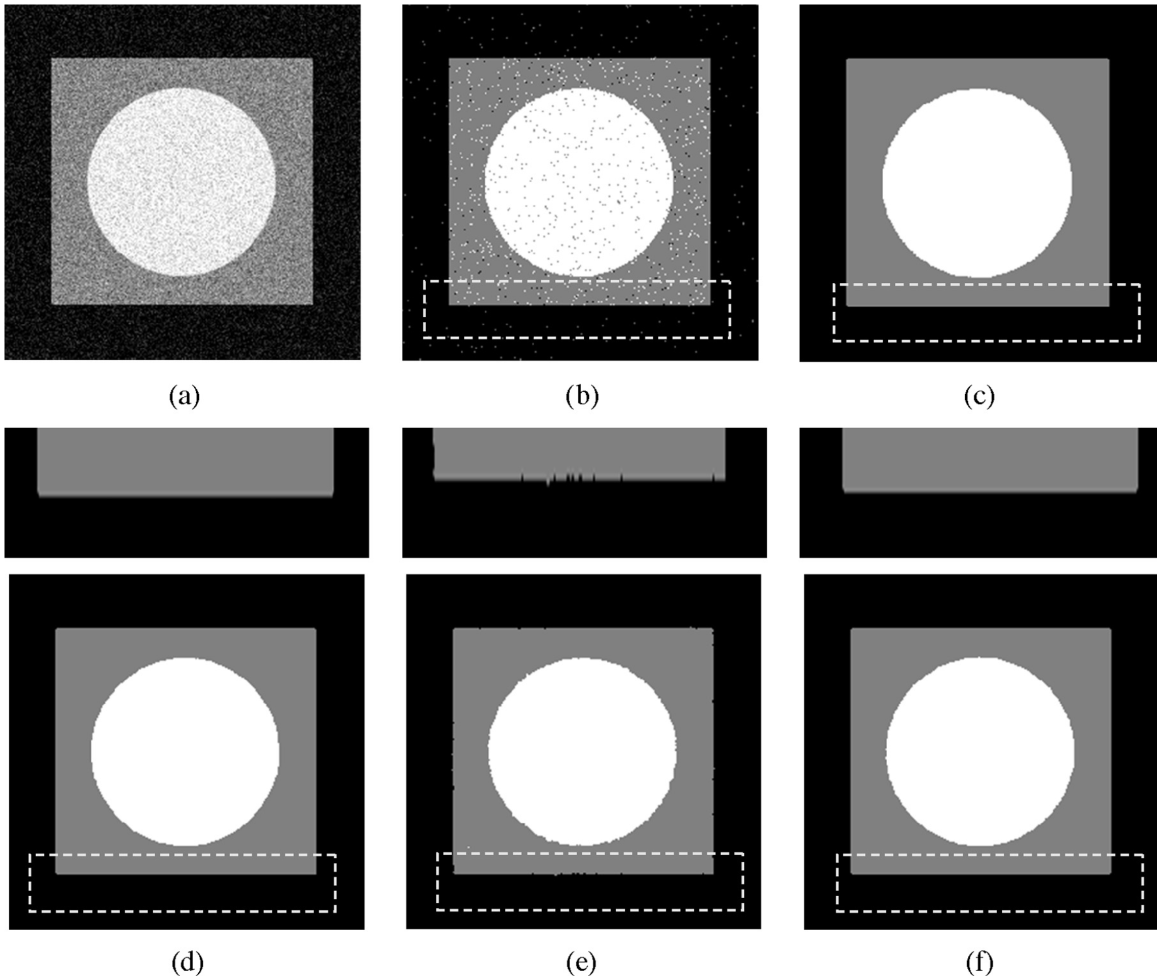

Fig. 4 – Segmentation of noisy synthetic image (noise variance 0.03): (a) noisy image segmented by (b) FCM, (c) sFCM, (d) sFCMM, (e) FLICM, and (f) the proposed IGFCM algorithm.

and the main liver tissues. For a segmentation to be ranked as high quality, the tumor must stand out of other two segments in the image. The original image and the resultant segmented images obtained after applying different segmentation algorithms on original image are shown in Fig. 7(a–f). The over-segmentation is immediately visible in case of segmentation produced by FCM, sFCM and sFCMM techniques. While, in case of FLICM segmentation, several misclassified patterns are observed in the tumor regions, as shown in Fig. 7(e). However, the proposed IGFCM segments tumor regions with high accuracy. The quantitative segmentation performance measures have also been computed by applying different segmentation techniques to noisy versions of the CT liver image. The proposed IGFCM outperforms all mentioned techniques at various noise levels as shown in Table 1.

3.1.4. *Quantitative analysis*

Table 1 compares the PC and CE measures for different segmentation techniques applied to noisy and noise-free images discussed in previous sections. Note that the quantitative results for carotid artery image correspond to the image shown in Fig. 9. The quantitative results in Table 1 indicate better segmentation using IGFCM than standard FCM and its variants. Particularly, there is a significant improvement in overall segmentation quality when input images contain noise of different levels. An exception is the case of synthetic image where sFCM and the proposed approach to produce comparable results. Also, the visual inspection of Figs. 2–4(c and f) reveals that the results of sFCM and IGFCM segmentation are comparable. However, IGFCM performs much better for other types of images. Hence, the general superiority of IGFCM is not lost.

The performance of different segmentation techniques, in terms of PC and CE, has also been compared graphically. As shown in Fig. 8, the results have been displayed only for the CT Liver image for demonstration purpose. In terms of both PC and CE measures, superiority of the proposed IGFCM algorithm is immediately evident from respective graphs. The performance advantage is even more in case of CE as compared to PC. Hence, it can be concluded reasonably that IGFCM performs better segmentation than FCM and its variants, especially in the presence of noise.

3.1.5. *Memory/computational analysis*

The storage and computational complexity of a segmentation technique is an important consideration, especially

Table 1 – Clustering quality comparison of various segmentation techniques.

	Partitioning coefficient (PC)				Classification entropy (CE)			
	Original	var .01	var .02	var .03	Original	var .01	var .02	var .03
Synthetic image								
FCM	–	0.9667	0.9659	0.9657	–	0.0702	0.0714	0.0721
sFCM	–	**0.9918**	**0.9916**	**0.9915**	–	**0.0135**	**0.0140**	**0.0142**
sFCMM	–	0.9913	0.9912	0.9911	–	0.0140	0.0143	0.0147
FLICM	–	0.8866	0.8446	0.8107	–	0.2485	0.3237	0.3811
The proposed IGFCM	–	0.9915	0.9914	0.9912	–	0.0138	0.0142	0.0145
The Wolf image								
FCM	0.9660	0.9655	0.9648	0.8800	0.1000	0.1201	0.1441	0.1810
sFCM	0.9831	0.9827	0.9815	0.9807	0.0164	0.0280	0.0296	0.0349
sFCMM	0.9840	0.9588	0.9543	0.9497	0.0195	0.0740	0.0820	0.0903
FLICM	0.9600	0.8724	0.8200	0.7906	0.1032	0.2663	0.3523	0.3984
The proposed IGFCM	**0.9847**	**0.9833**	**0.9823**	**0.9812**	**0.0142**	**0.0200**	**0.0284**	**0.0314**
Liver CT								
FCM	0.9251	0.8300	0.8100	0.8000	0.1370	0.3000	0.3000	0.3200
sFCM	0.9355	0.8670	0.8662	0.8627	0.1201	0.2345	0.2357	0.2417
sFCMM	0.9380	0.9041	0.9001	0.8891	0.1559	0.2013	0.2130	0.2388
FLICM	0.9417	0.7384	0.6625	0.6150	0.1015	0.4843	0.6037	0.6767
The proposed IGFCM	**0.9451**	**0.9123**	**0.9013**	**0.8910**	**0.1002**	**0.1401**	**0.1500**	**0.1633**
Carotid artery ultrasound image (Fig. 9)								
FCM	0.7850	0.7735	0.7509	0.7297	0.3719	0.3886	0.4109	0.4373
sFCM	0.8461	0.8209	0.7891	0.7722	0.2850	0.3162	0.3409	0.3796
sFCMM	0.8662	0.8409	0.8202	0.7980	0.2150	0.2594	0.2773	0.2862
FLICM	0.8000	0.7566	0.7141	0.6803	0.3833	0.4580	0.5267	0.5799
The proposed IGFCM	**0.8873**	**0.8497**	**0.8364**	**0.8145**	**0.1925**	**0.2472**	**0.2633**	**0.2686**

The text in bold-face notation represents the maximum performance for a particular image among various techniques.

when two competitor methods have very similar segmentation results. The proposed IGFCM algorithm does not require any additional storage capacity as no memory-intensive data structure has been introduced. Similarly, the computational performance of the proposed algorithm is also comparable to other employed fuzzy algorithms except FCM. However, FCM suffers intensively in the presence of noise; therefore, its computational superiority is not justifiable. All other employed

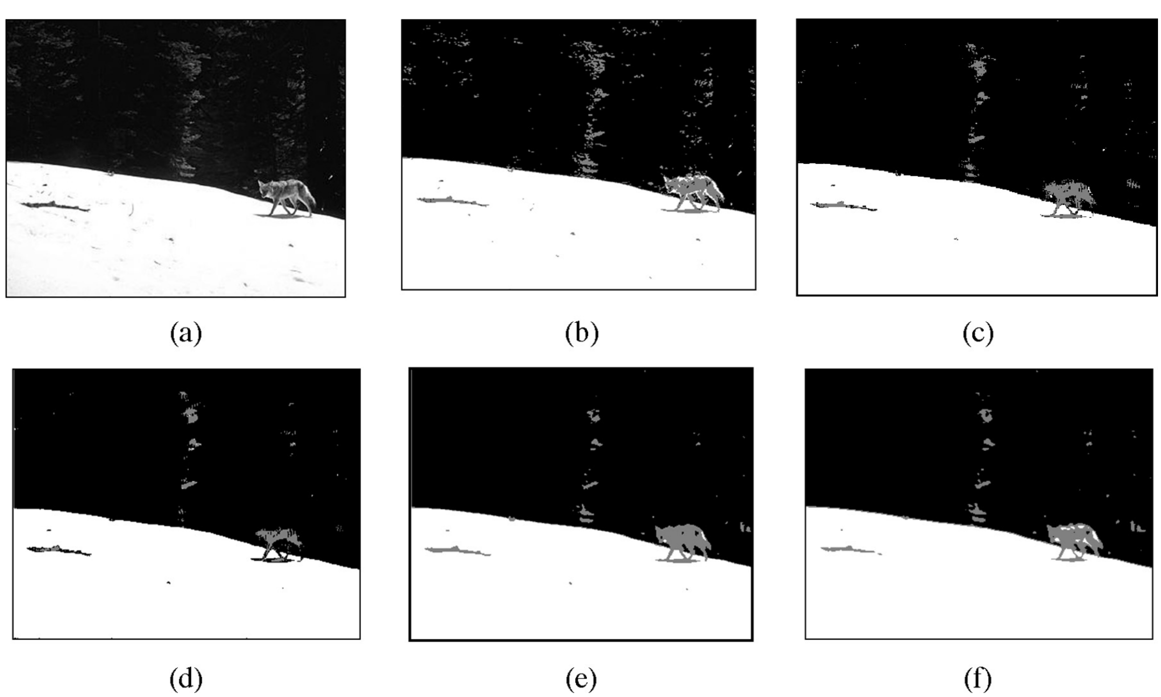

Fig. 5 – The Wolf image segmentation, (a) The Wolf image (original), (b) FCM segmentation, (c) sFCM segmentation, (d) sFCMM segmentation, (e) FLICM segmentation, and (f) the proposed IGFCM segmentation.

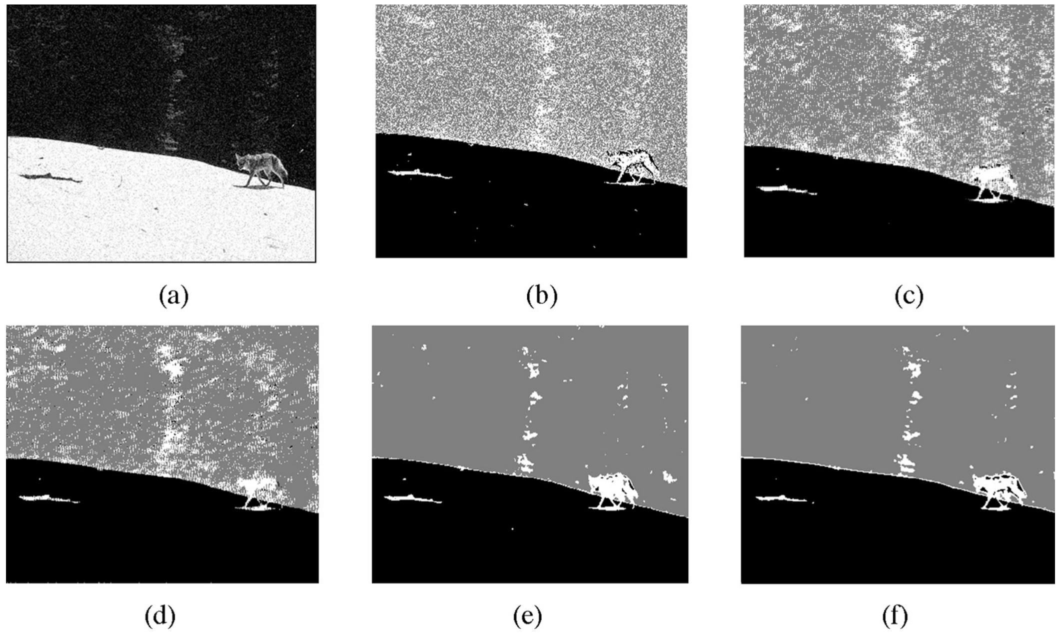

Fig. 6 – Segmentation of noisy Wolf image (noise variance 0.01), (a) noisy Wolf image, (b) FCM segmentation, (c) sFCM segmentation, (d) sFCMM segmentation, (e) FLICM segmentation, and (f) the proposed IGFCM segmentation.

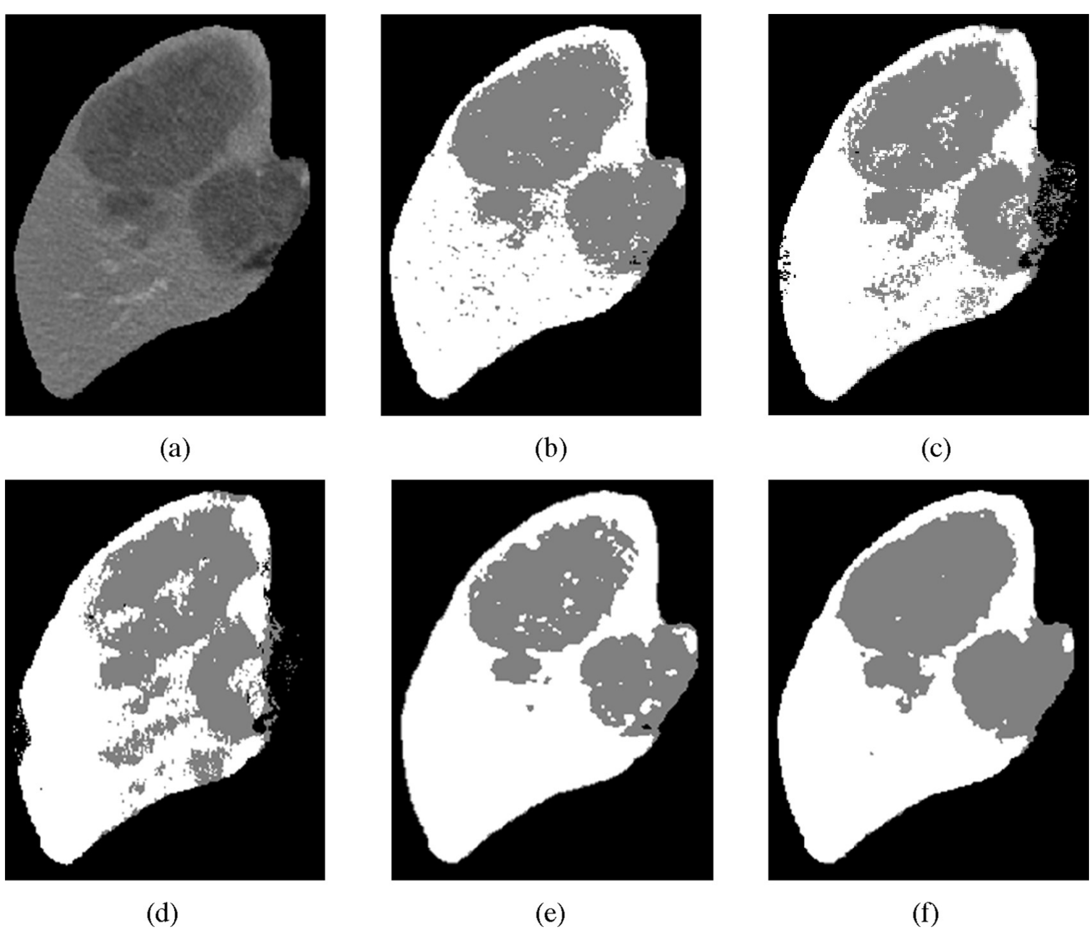

Fig. 7 – CT liver image segmentation, (a) original CT liver image, (b) FCM segmentation, (c) sFCM segmentation, (d) sFCMM segmentation, (e) FLICM segmentation, and (f) the proposed IGFCM segmentation.

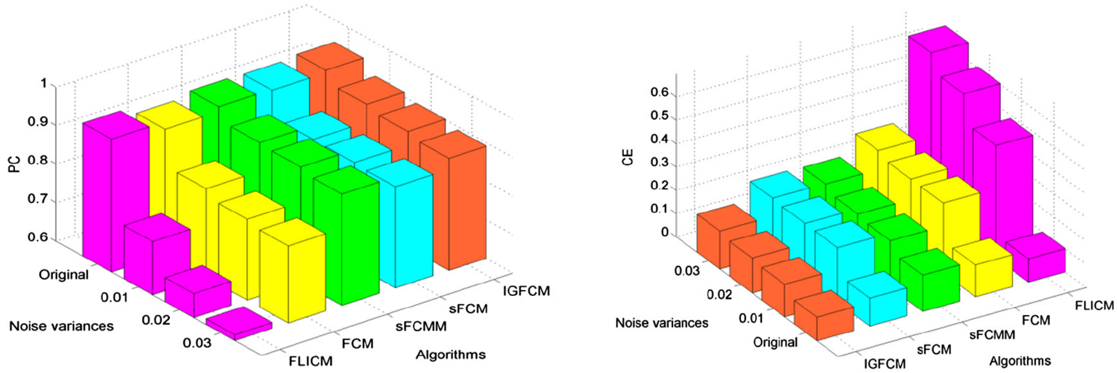

(a) PC measure for CT Liver image.

(b) CE measure for CT Liver image.

Fig. 8 – Graphical comparison of clustering quality measures for the CT Liver image.

fuzzy algorithms process the input image in a way similar to IGFCM i.e. they convolve the input image with a window of certain size. Moreover, due to the information induced by information gain in the convergence process, the proposed IGFCM algorithm converges in less number of iterations than other algorithms. The computation of information gain is an additional step in the proposed algorithm. However, the cost of computing information gain is balanced by faster convergence rate of IGFCM. Finally, in several offline medical applications, segmentation accuracy is the main concern rather than computational complexity. Therefore, our technique is preferable to other techniques as the segmentation accuracy results presented in the paper verify its superiority.

As an improvement to the proposed IGFCM algorithm from computational perspective, we conjecture that a parallel implementation similar to [34] is also possible. Authors have presented a non-rigid 3D medical image registration framework and a high-speed GPU-based parallel implementation of the framework has also been proposed. The GPU-based implementation of FCM is also part of this framework. The proposed IGFCM approach is consistent with the FCM implementation presented in [34]. Parallel implementation of FCM in [34] spreads the processing across several kernels, each one performing certain processing. Different steps involved in the proposed IGFCM technique can also be parallelized in a similar way. Ideally, additional kernel(s) may be introduced related to the computation of information gain. Hence, the GPU-based implementation may drastically increase the computational performance of the proposed IGFCM algorithm.

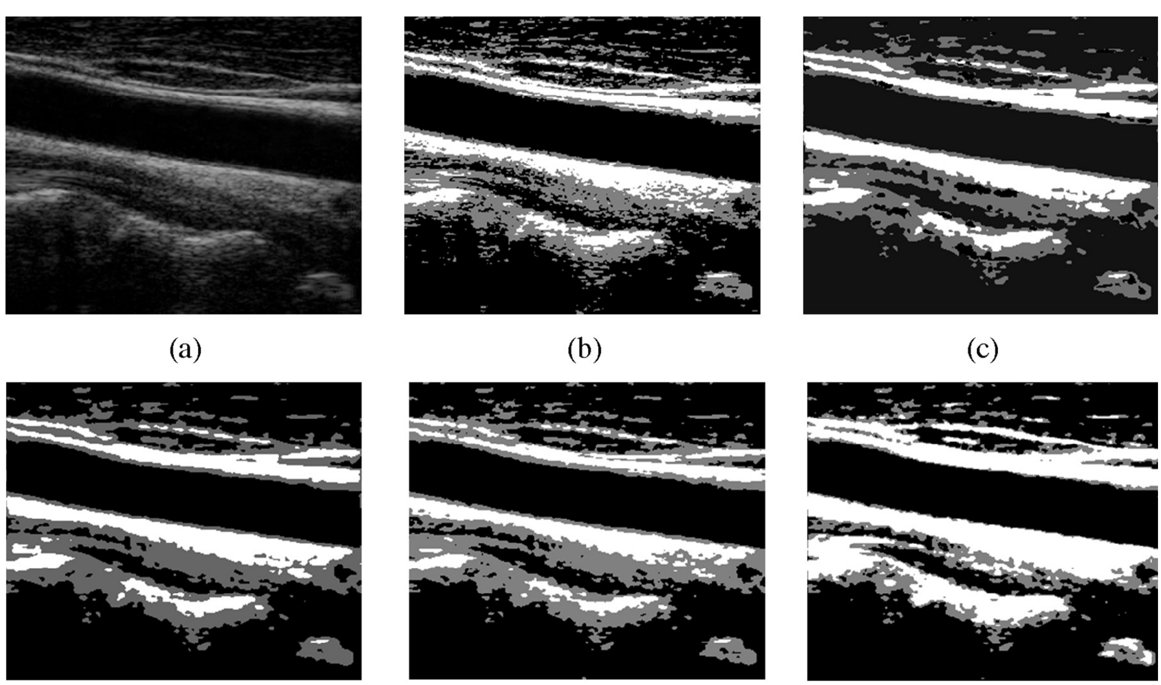

(a) (b) (c)

(d) (e) (f)

Fig. 9 – Carotid artery US image segmentation, (a) original carotid artery US image, (b) FCM segmentation, (c) sFCM segmentation, (d) sFCMM segmentation, (e) FLICM segmentation, and (f) the proposed IGFCM segmentation.

(a) Original carotid artery ultrasound image

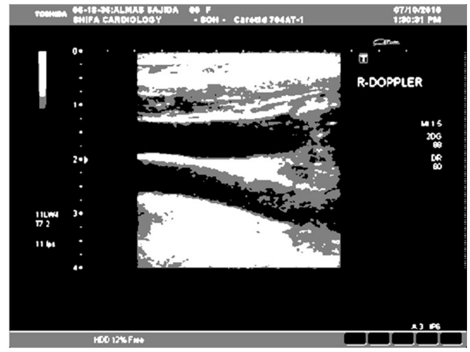

(b) IGFCM segmentation

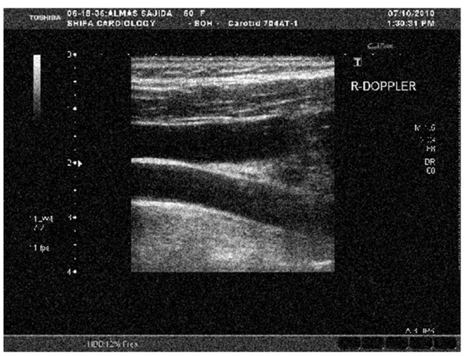

(c) Gaussian noise of variance 0.01

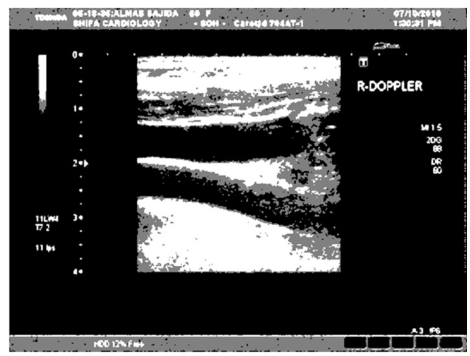

(d) IGFCM segmentation

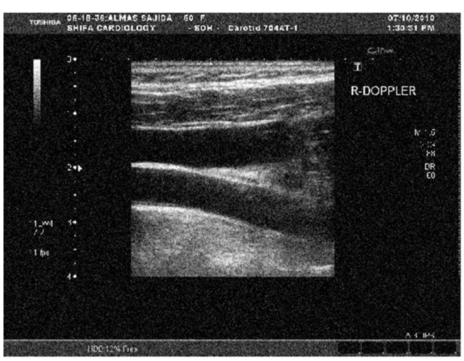

(e) Gaussian noise of variance 0.02

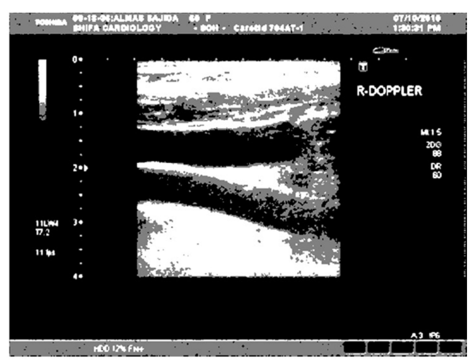

(f) IGFCM segmentation

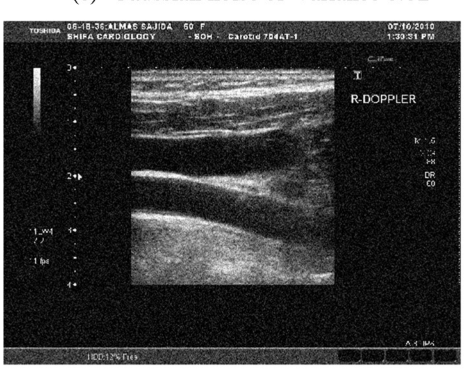

(g) Gaussian noise of variance 0.03

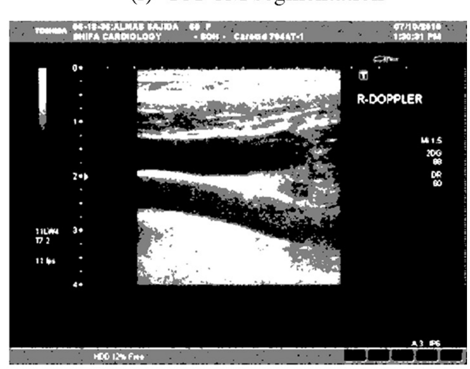

(h) IGFCM segmentation

Fig. 10 – IGFCM segmentation at noise free and noisy carotid artery ultrasound image corrupted through Gaussian noise of various intensities.

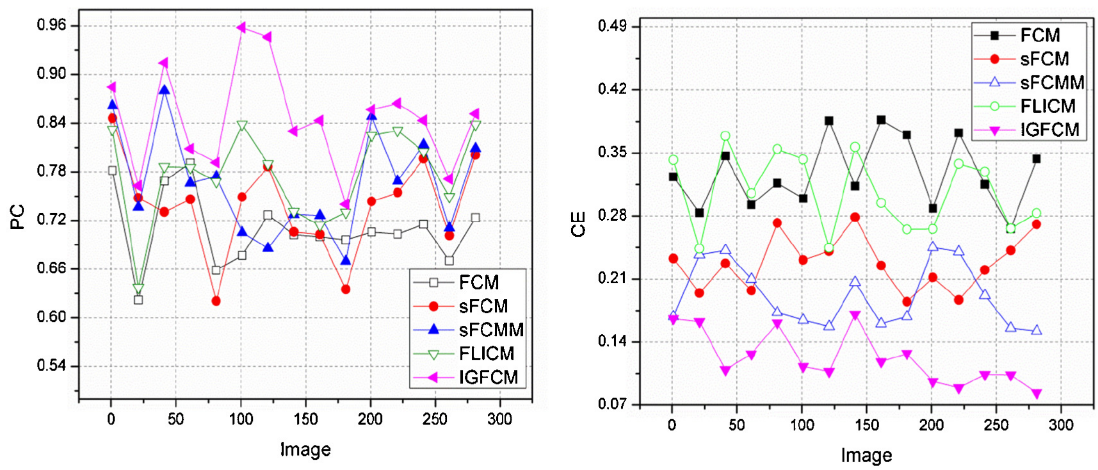

a) The PC measure b) The CE measure

Fig. 11 – The PC and CE measure of 300 carotid artery ultrasound images.

3.2. *Scenario 2: segmentation and decision performance on carotid artery ultrasound images*

In the second scenario, the proposed technique is applied to segment a dataset (see Section 2.1) of 300 carotid artery ultrasound images. Ultrasound (US) is one of the most commonly used medical imaging modality. A large number of applications of US in medical imagery are due to its radiation-safe and cost-effective operation. We have segmented carotid artery ultrasound images using FCM, sFCM, sFCMM, FLICM and the proposed IGFCM into three clusters namely the arterial wall, an area inside the artery and the background tissues. Fig. 9(a) shows region of interest (ROI) for one of the original carotid artery ultrasound images. Fig. 9(b–e) shows that in all cases the FCM and its variants have produced clustering with misclassified pixels. The IGFCM segmented image, on the other hand, produces homogenous clustering, as shown in Fig. 9(f).

A keen observation of Fig. 9 reveals that images segmented by variants of FCM contain more misclassified pixels in the background and arterial walls regions. Misclassification of arterial wall tissues cannot be tolerated as accurate IMT values are directly dependent on accurate segmentation of arterial wall. On the other hand, the image segmented by IGFCM has fewer misclassified pixels at arterial walls and background area compared to other techniques. Fig. 10 shows the proposed approach segmentation at various intensities of Gaussian noise. It can be seen from Fig. 10 that the proposed IGFCM has successfully segmented carotid artery ultrasound image. Further, very few misclassifications show the robustness of the IGFCM approach.

Fig. 11(a) and (b) shows PC and CE measures for various carotid artery images from the database of 300 images. For convenient comparison, the results have been shown on an interval of 15 images, resulting into 20 images. The PC and CE measures for the whole dataset of carotid artery ultrasound images are also presented in supplementary material (see Figs. 1 and 2, Tables 2 and 3). However, average results for all 300 images are also compared for different segmentation techniques in Fig. 12. The results in Figs. 11 and 12 verify that the proposed IGFCM approach outperforms other variants of FCM. The proposed IGFCM approach also yields more consistent results as evident by the standard deviation values in Fig. 12.

A decision system for classification of carotid artery ultrasound images into normal/abnormal subjects has also been proposed in this work. The classification is performed based on features computed from IMT values which, in turn, are measured from segmented carotid artery images. Precise IMT measurement is based on accurate segmentation which, consequently, yields a better decision accuracy. Therefore, for our proposed decision making system, the IMT values have been measured from the carotid artery US images segmented by IGFCM algorithm.

IMT values for upper and lower carotid artery walls have been measured, with the help of a medical expert, from each segmented image. Fig. 13 shows the measured IMT curve for one of the normal and abnormal carotid artery ultrasound images, respectively. IMT mean and standard deviation of the

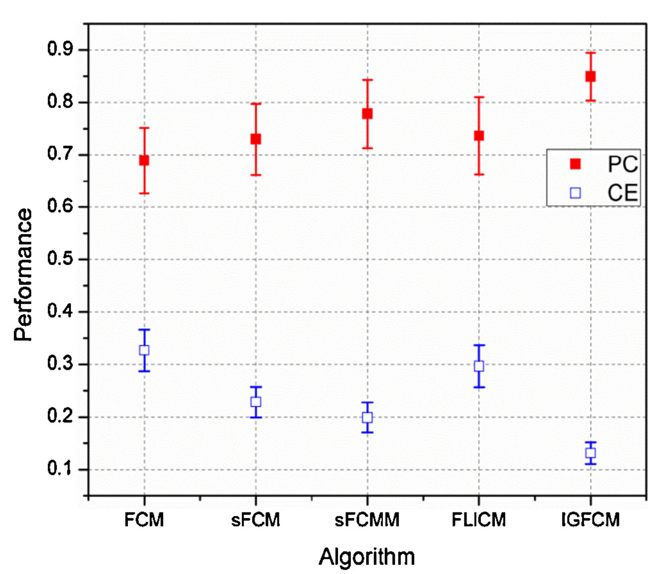

Fig. 12 – Average PC and CE measures for 300 carotid artery ultrasound images.

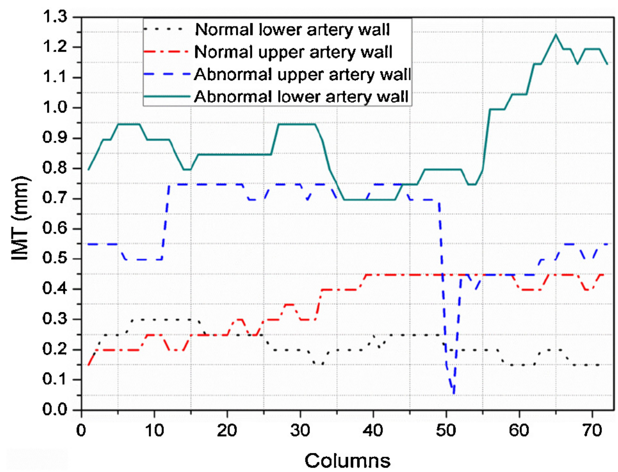

Fig. 13 – Normal and abnormal IMT measurements of a carotid artery.

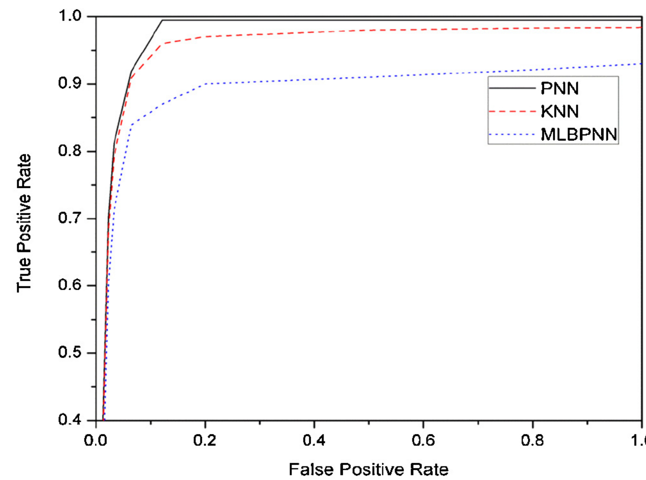

Fig. 14 – ROC curve plotted against true positive rate vs. false positive rate for PNN, KNN and MLBPNN.

normal carotid artery are 0.3824 mm and 0.1046 mm, respectively, and for the abnormal carotid artery mean and standard deviation are 0.7630 mm and 0.1702 mm, respectively. A feature vector comprising 6 features (see Section 2.4) has been constructed from IMT values and fed as input to the PNN classifier for training and validation.

The decision performance of different classifiers based on the proposed segmentation technique has been compared. Table 2 shows the performance comparison in terms of different quantitative measures for PNN, KNN and MLBPNN classifiers. Chaudhry et al. [10] reported 98.10% and Santhiyakumari et al. [35] obtained 96% classification accuracy on their datasets. While, using images segmented by our proposed technique, 98.40% classification accuracy has been achieved using PNN classifier. Hence, the positive influence of our proposed technique on the classification process is evident.

Fig. 14 shows ROC curves for PNN, KNN, MLBPNN classifiers. It can be observed from Fig. 14 that the ROC curve of PNN is close to vertical axis which signifies that there are fewer misclassifications compared to KNN and MLBPNN. The AUC value for PNN has been computed as 0.982 which indicates high diagnostic accuracy. These statistical results indicate that the proposed decision system has effectively discriminated the abnormal subjects from normal one.

Finally, we have also compared the effect of different segmentation techniques on classification performance. In particular, FCM, sFCM, sFCMM, FLICM and IGFCM have been applied to 300 carotid artery images and segmented images have been classified using PNN, KNN and MLBPNN classifiers.

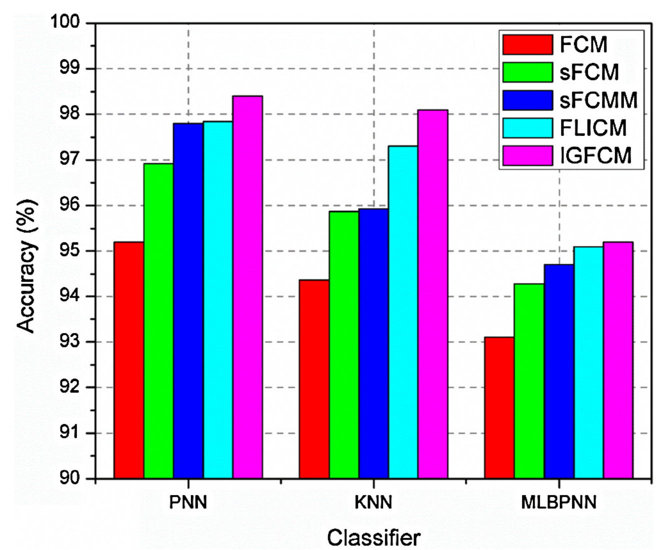

Fig. 15 – Effect of segmentation techniques on the classification of carotid artery images.

Fig. 15 shows that highest classification accuracy is obtained by segmenting carotid artery ultrasound images using IGFCM and classifying through PNN classifier which we suggested in our proposed decision system.

Critically analyzing the classification results presented in Fig. 15, one can observe that classification accuracy is improved by 3.27%, 3.80% and 4.31%, respectively, for PNN, KNN and MLBPNN classifiers (see Table 1 in supplementary

Table 2 – Performance comparison of PNN-based decision system with other classifiers.

Classifiers	Classification validity measures				
	Accuracy (%)	MCC	F-score	Sensitivity	Specificity
PNN	98.40	0.9600	0.9799	0.9839	0.9762
KNN	98.10	0.9520	0.9709	0.9742	0.9725
MLBPNN	95.20	0.8600	0.9244	0.9735	0.8905

material). This significant classification improvement is due to the accurate segmentation of carotid artery ultrasound images by the proposed IGFCM technique. As the classification phase is dependent on correct IMT measurements which is derived from accurate segmentation. Hence, it can be concluded that the proposed segmentation based classification scheme can successfully be applied to identify the presence of plaque in carotid artery.

Hence, the proposed IGFCM algorithm boosts classification accuracy and can be used as part of the proposed decision system.

4. Conclusions

In this paper, a robust technique, called IGFCM, has been proposed for segmentation of medical images. The conventional FCM algorithm is associated with high noise susceptibility and non homogeneous clustering. The proposed algorithm incorporates the concept of information gain into fuzzy framework in order to overcome the shortcomings of conventional FCM algorithm. It updates the fuzzy membership values of a pixel based on its information gain computed from pixels in its local neighborhood. The proposed IGFCM algorithm has been applied to segment images from different modalities and compared with conventional FCM and three different variants of FCM. Gaussian noise of various intensities is added to the images in order to check robustness of the proposed technique. Quantitative measures (PC and CE), computed from segmented images from different modalities, verify the robustness and effectiveness of the proposed algorithm over other techniques.

Afterwards, a decision system has been designed based on PNN classifier using a dataset of 300 real carotid artery ultrasound images. The proposed decision system has successfully distinguished the abnormal subjects from normal ones with accuracy of 98.40%. In addition to this, effect of segmentation on classification has also been investigated. The classification accuracy based on the proposed segmentation technique has been improved by 3.27% compared to other segmentation techniques using PNN classifier. The significant improvement in classification accuracy is due to accurate segmentation of carotid artery ultrasound images by the proposed IGFCM approach. Hence, it is expected that the proposed technique can be used effectively in a decision system to detect the plaque in carotid artery and can assist the radiologists as a secondary decision maker.

Acknowledgements

This research work is supported by the Higher Education Commission of Pakistan under the indigenous PhD scholarship program (17-5-4(Ps4-078)/HEC/Sch/2008/). The authors would like to extend their thanks to Shifa International Hospital, Islamabad for providing the data and technical support to complete this research work.

Appendix A. Supplementary data

Supplementary data associated with this article can be found, in the online version, at http://dx.doi.org/10.1016/j.cmpb.2013.10.012.

REFERENCES

[1] D. Velakoulis, S.J. Wood, W.M.H. Wong, P.D. McGorry, A. Yung, et al., Hippocampal and amygdala volumes according to psychosis stage and diagnosis: a magnetic resonance imaging study of chronic schizophrenia, first-episode psychosis, and ultra-high-risk individuals, Archives of General Psychiatry 63 (2006) 139–149.

[2] A. Chaudhry, M. Hassan, A. Khan, J.Y. Kim, T.A. Tuan, Image clustering using improved spatial fuzzy C-means, in: Proceedings of the Sixth International Conference on Ubiquitous Information Management and Communication, ACM, Kuala Lumpur, Malaysia, 2012.

[3] S.M. Smith, P.T. Fox, K.L. Miller, D.C. Glahn, P.M. Fox, C.E. Mackay, N. Filippini, K.E. Watkins, R. Toro, A.R. Laird, C.F. Beckmann, Correspondence of the brain's functional architecture during activation and rest, Proceedings of the National Academy of Sciences 106 (2009) 13040–13045.

[4] J. Tan, D. Lim Joon, G. Fitt, M. Wada, M. Lim Joon, A. Mercuri, M. Marr, M. Chao, V. Khoo, The utility of multimodality imaging with CT and MRI in defining rectal tumour volumes for radiotherapy treatment planning: a pilot study, Journal of Medical Imaging and Radiation Oncology 54 (2010) 562–568.

[5] N. Ayache, P. Cinquin, I. Cohen, L. Cohen, F. Leitner, O. Monga, Segmentation of complex three dimensional medical objects: a challenge and a requirement for computer-assisted surgery planning and performance, Computer Integrated Surgery: Technology and Clinical Applications (1996) 59–74.

[6] M. Kamel, A. Campilho, A.R. Abdel-Dayem, M.R. El-Sakka Senior Member Ieee, Carotid artery ultrasound image segmentation using fuzzy region growing, in: Image Analysis and Recognition, Springer, Berlin/Heidelberg, 2005, pp. 869–878.

[7] W. Li, P. Ogunbona, C. deSilva, Y. Attikiouzel, Semi-supervised maximum a posteriori probability segmentation of brain tissues from dual-echo magnetic resonance scans using incomplete training data, IET Image Processing 5 (2011) 222–232.

[8] N. Karimi, S. Samavi, S. Shirani, P. Behnamfar, Segmentation of DNA microarray images using an adaptive graph-based method, IET Image Processing 4 (2010) 19–27.

[9] B. Caldairou, N. Passat, P.A. Habas, C. Studholme, F. Rousseau, A non-local fuzzy segmentation method: application to brain MRI, Pattern Recognition 44 (2011) 1916–1927.

[10] A. Chaudhry, M. Hassan, A. Khan, J. Kim, T. Tuan, Automatic segmentation and decision making of carotid artery ultrasound images Intelligent Autonomous Systems, vol. 12, Springer, Berlin Heidelberg, 2012, pp. 185–196.

[11] M. Kamel, A. Campilho, A. Abdel-Dayem, M. El-Sakka, Fuzzy c-means clustering for segmenting carotid artery ultrasound images, in: Image Analysis and Recognition, Springer, Berlin/Heidelberg, 2007, pp. 935–948.

[12] R. Rui, Aur, C. lio, S. Jorge, A. Elsa, S. Rosa, Segmentation of ultrasound images of the carotid using RANSAC and cubic

splines, Computer Methods and Programs in Biomedicine 101 (2011) 94–106.
[13] H. Zaidi, Medical image segmentation: Quo Vadis, Computer Methods and Programs in Biomedicine 84 (2006) 63–65.
[14] F. Latifoglu, K. Polat, S. Kara, S. Gunes, Medical diagnosis of atherosclerosis from Carotid Artery Doppler Signals using principal component analysis (PCA), k-NN based weighting pre-processing and Artificial Immune Recognition System (AIRS), Journal of Biomedical Informatics 41 (2008) 15–23.
[15] S. Krinidis, V. Chatzis, A robust fuzzy local information c-means clustering algorithm, IEEE Transactions on Image Processing 19 (2010) 1328–1337.
[16] J. Richard, S. Qiang, Computational Intelligence and Feature Selection: Rough and Fuzzy Approaches, Wiley-IEEE Press, 2008.
[17] K.-S. Chuang, H.-L. Tzeng, S. Chen, J. Wu, T.-J. Chen, Fuzzy c-means clustering with spatial information for image segmentaion, Computerized Medical Imaging and Graphics 30 (2006) 9–15.
[18] W. Cai, S. Chen, D. Zhang, Fast and robust fuzzy c-means clustering algorithms incorporating local information for image segmentation, Pattern Recognition 40 (2007) 825–838.
[19] T. Kiatichai, J. Chuleerat, Entropy based fuzzy c-mean for item-based collaborative filtering, in: Proceedings of the 9th International Conference on Communications and Information Technologies, IEEE Press, Incheon, Korea, 2009.
[20] A.L. Barbieri, G.F. de Arruda, F.A. Rodrigues, O.M. Bruno, L.d.F. Costa, An entropy-based approach to automatic image segmentation of satellite images, Physica A: Statistical Mechanics and its Applications 390 (2011) 512–518.
[21] S.L. Murphy, J. Xu, K.D. Kochanek, National Vital Statistics Report, National Center for Health Statistics, Hyattsville, 2013.
[22] Stroke, National Institute of Health, 2012 http://www.nlm.nih.gov/medlineplus/ency/article/000726.htm
[23] F. Mao, J. Gill, D. Downey, A. Fenster, Segmentation of carotid artery in ultrasound images, in: Proceedings of the 22nd Annual International Conference of the IEEE Engineering in Medicine and Biology Society, 2000, pp. 1734–1737.
[24] C.P. Loizou, C.S. Pattichis, M. Pantziaris, A. Nicolaides, An integrated system for the segmentation of atherosclerotic carotid plaque, IEEE Transactions on Information Technology in Biomedicine 11 (2007) 661–667.
[25] M. Hassan, C. Asmatullah, K. Asifullah, K. Jin Young, Carotid artery image segmentation using modified spatial fuzzy c-means and ensemble clustering, Computer Methods and Programs in Biomedicine 108 (2012) 1261–1276.
[26] N. Tsiaparas, S. Golemati, I. Andreadis, J.S. Stoitsis, I. Valavanis, K.S. Nikita, Comparison of multiresolution features for texture classification of carotid atherosclerosis from B-mode ultrasound, Transactions on Information Technology and Biomedicine 15 (2011) 130–137.
[27] E.C. Kyriacou, S. Petroudi, C.S. Pattichis, M.S. Pattichis, M. Griffin, S. Kakkos, A. Nicolaides, Prediction of high-risk asymptomatic carotid plaques based on ultrasonic image features, IEEE Transactions on Information Technology in Biomedicine 16 (2012) 966–973.
[28] C.E. Shanoon, A mathematical theory of communication, Bell System Technical Journal 27 (1948) 379–423.
[29] M. Filippo, Z. Guang, S.S. Jasjit, Review: a state of the art review on intima-media thickness (IMT) measurement and wall segmentation techniques for carotid ultrasound, Computer Methods and Programs in Biomedicine 100 (2012) 201–221.
[30] M. Filippo, M.M. Kristen, S. Luca, U.R. Acharya, L. Giuseppe, Z. Guang, H. Sin Yee Stella, T.A. Anil, C.H. Suzanne, N. Andrew, S.S. Jasjit, Ultrasound IMT measurement on a multi-ethnic and multi-institutional database: our review and experience using four fully automated and one semi-automated methods, Computer Methods and Programs in Biomedicine 108 (2012) 946–960.
[31] A. Chaudhry, M. Hassan, A. Khan, J. Kim, Automatic active contour-based segmentation and classification of carotid artery ultrasound images, Journal of Digital Imaging (2013) 1–11, http://dx.doi.org/10.1007/s10278-012-9566-3.
[32] F.S. Donald, Probabilistic neural networks, Neural Networks 3 (1990) 109–118.
[33] S.H. Park, J.M. Goo, C.-H. Jo, Receiver operating characteristic (ROC) curve: practical review for radiologists, Korean Journal of Radiology 5 (1) (2004) 11–18.
[34] R. Gallea, E. Ardizzone, R. Pirrone, O. Gambino, Three-dimensional Fuzzy Kernel Regression framework for registration of medical volume data, Pattern Recognition 46 (2013) 3000–3016.
[35] N. Santhiyakumari, P. Rajendran, M. Madheswaran, Medical decision-making system of ultrasound carotid artery intima-media thickness using neural networks, Journal of Digital Imaging 24 (2011) 1112–1125.